Rigorous coupled-wave analysis of electromagnetic scattering from lamellar grating with defects

Koki Watanabe,[1,2,*] **Jaromír Pištora,**[2] **and Yoshimasa Nakatake**[3]

[1] *Department of Information and Communication Engineering, Fukuoka Institute of Technology, 3-30-1 Wajirohigashi, Higashi-ku, Fukuoka 811-0295, Japan*
[2] *Nanotechnology Centre, VŠB-Technical University of Ostrava, 17. listopadu 15, 708 33 Ostrava-Poruba, Czech Republic*
[3] *Graduate School of Engineering, Fukuoka Institute of Technology, 3-30-1 Wajirohigashi, Higashi-ku, Fukuoka 811-0295, Japan*
**koki@fit.ac.jp*

Abstract: This paper proposes a spectral-domain approach to the electromagnetic scattering problem of lamellar grating with defects. The fields in imperfectly periodic structures have continuous spectra in the wavenumber space, and the main problem of the spectral-domain approach is connected to the discretization scheme on the wavenumber. The present approach introduces the pseudo-periodic Fourier transform to consider the discretization scheme in the Brillouin zone. This transformation also makes it possible to apply the conventional grating formulations to the problems of imperfectly periodic structures. The present formulation is based on the rigorous coupled-wave analysis with the help of pseudo-periodic Fourier transform.

OCIS codes: (050.0050) Diffraction and gratings; (050.1755) Computational electromagnetic methods; (050.1950) Diffraction gratings.

References and links

1. O. Manyardo, R. Michaely, F. Schädelin, W. Noell, T. Overstolz, N. De Rooij, H. P. Herzig, "Miniature lamellar grating interferometer based on silicon technology," Opt. Lett. **29,** 1437–1439 (2004).
2. Y. Hongbin, Z. Guangya, Ch. F. Siong, L. Feiwen, W. Shouhua, Z. Mingsheng, "An electromagnetically driven lamellar grating based Fourier transform microspectrometer," J. Micromech. Microeng. **18,** 055016 (2008).
3. A. Sato, "Analysis of finite-sized guided-mode resonant gratings using the fast multipole boundary element method," J. Opt. Soc. Am. A **27,** 1909–1919 (2010).
4. F. Marquier, C. Arnold, M. Laroche, J. J. Greffet, Y. Chen, "Degree of polarization of thermal light emitted by gratings supporting surface waves," Opt. Express **16,** 5305–5313 (2008).
5. N. Bonod, G. Tayeb, D. Maystre, S. Enoch, E. Popov, "Total absorption of light by lamellar metallic gratings," Opt. Express **16,** 15431–15438 (2008).
6. W. T. Lu, Y. J. Huang, P. Vodo, R. K. Banyal, C. H. Perry, S. Sridhar, "A new mechanism for negative refraction and focusing using selective diffraction from surface corrugation," Opt. Express **15,** 9166–9175 (2007).
7. L. Pajewski, R. Borghi, G. Schettini, F. Frezza, M. Santarsiero, "Design of a binary grating with subwavelength features that acts as a polarizing beam splitter," Appl. Opt. **40,** 5898–5905 (2001).
8. T. Käpfe, O. Parriaux, "Parameter-tolerant binary gratings," J. Opt. Soc. Am. A **27,** 2660–2669 (2010).
9. T. Oonishi, T. Konishi, K. Itoh, "Fabrication of phase only binary blazed grating with subwavelength structures designed by deterministic method based on electromagnetic analysis," Jpn. J. Appl. Phys. **46,** 5435–5440 (2007).
10. R. Antoš, J. Pištora, I. Ohlídal, K. Postava, J. Mistrík, T. Yamaguchi, Š. Višňovský, M. Horie, "Specular spectroscopic ellipsometry for the critical dimension monitoring of gratings fabricated on a thick transparent plate," J. Appl. Phys. **97,** 053107 (2005).

11. W. Nakagawa, P.-Ch. Sun, Ch-H. Chen, Y. Fainman, "Wide-field-of-view narrow-band spectral filters based on photonic crystal nanocavities," Opt. Lett. **27,** 191–193 (2002).
12. B. G. Zhai, Y. G. Cai, Y. M. Huang, "Transmission spectra of one-dimensional photonic crystal with a centered defect," Mat. Sci. For. **663–665,** 733–736 (2010).
13. K. Ren, X. Ren, R. Li, J. Zhou, D. Liu, "Creating "defects" in photonic crystals by controlling polarizations," Phys. Lett. **325,** 415–419 (2004).
14. E. G. Loewen and E. Popov, *Diffraction Gratings and Applications* (Marcel Dekker, New York, 1997).
15. K. Watanabe and K. Yasumoto, "Two-dimensional electromagnetic scattering of non-plane incident waves by periodic structures," Progress in Electromagnetic Res. **PIER 74,** 241–271 (2007).
16. R. Petit, ed., *Electromagnetic Theory of Gratings* (Springer-Verlag, Berlin, 1980).
17. K. Knop, "Rigorous diffraction theory for transmission phase gratings with deep rectangular grooves," J. Opt. Soc. Am. **68,** 1206–1210 (1978).
18. M. G. Moharam and T. K. Gaylord, "Diffraction analysis of dielectric surface-relief gratings," J. Opt. Soc. Am. **72,** 1385–1392 (1982).
19. L. Li, "Use of Fourier series in the analysis of discontinuous periodic structures," J. Opt. Soc. Am. A **13,** 1870–1876 (1996).
20. K. Watanabe and Y. Nakatake, "Spectral-domain formulation of electromagnetic scattering from circular cylinders located near periodic cylinder array," Prog. Electromagn. Res. B **31,** 219–237 (2011).
21. H. Takahasi and M. Mori, "Double exponential formulas for numerical integration," Publ. RIMS, Kyoto Univ. **9,** 721–741 (1974).
22. P. J. Davis and P. Rabinowitz, *Methods of Numerical Integration*, 2nd ed. (Academic Press, New York, 1984).

1. Introduction

Lamellar gratings are widely used for spectrographs, monochromators, laser tuning, integrated optics etc. Frequently, application is a lamellar grating interferometer (a binary grating with a variable depth) that operates in the zeroth order of the diffraction pattern [1]. In Ref. [2] a lamellar grating, in which an electromagnetic actuator used to drive the mobile facets of the lamellar grating to move bi-directionally, is described. The physical principle of wave front separation on grating requires the determinated lamellar geometry. The combination of planar waveguides with lamellar gratings enables us to create guided-mode resonant grating filters [3]. The resonant excitation of surface waves on a grating is known. New studies describe the influence of the role of angle and polarization on thermal emission by lamellar gratings [4]. Lamellar gratings can achieve, with suitable optogeometrical parameters, a total absorption of light. For the orthogonal polarization, total absorption occurs for deep gratings only [5]. The negative refraction is achieved by incorporating a surface grating on a flat multilayered material (grisms: grating-prisms). This negative refraction mechanism is used to create a new optical device, the grating lens [6]. The principle of suitably sized subwavelength groups etched in an isotropic dielectric medium is used in grating preparation, working on the first or the second diffraction order, depending on the polarization state of the incident radiation [7]. The solution to the problem of canceling the zeroth transmitted order in binary grating with a large tolerance on the corrugation duty cycle or a large spectral bandwidth is described in Ref. [8].

The fabrication of binary micro- and nanostructures has the potential to cause various defects. The specification of defects influence on the diffraction efficiency is very important. This effect, due to the fabrication process, has been described by a binary grating with subwavelength structures designed using design method [9]. It has been specified that the decrease in the diffraction efficiency is less than several percent in this case. The stripe grating profiles have been studied by spectral ellipsometry and the critical dimensions have been specified [10]. On the contrary, the defects are artificially generated to change the physical properties of periodical structures. In Ref. [2] a lamellar grating, in which an electromagnetic actuator is used to drive the mobile facets of the lamellar grating to move bi-directionally, is described. The principle of defects implementation is used in photonics crystals. The function of the defect's refractive index in spectral filters based on photonics crystal is analyzed in Ref. [11]. The one-dimensional photonic crystals with single defects in the center show the defect band gap in transmittance

spectra [12]. The defect mode in photonic crystal can be achieved by illuminating the structure with controlled polarizations [13].

This paper presents a rigorous numerical approach in the spectral-domain to the electromagnetic scattering problem from lamellar grating with defects. The fields in the structure with imperfect periodicity have continuous spectra in the wavenumber space, and an artificial discretization in the wavenumber space is necessary for the spectral-domain approach. When the plane-wave illuminates the perfectly periodic structures, rapid variations of the diffraction efficiencies are observed at discrete angles of incidence. These phenomena are known as the Wood anomalies [14]. Considering the Fourier integral representation of the fields, we may understand that the fields in the periodic structures are not smooth at the anomalies in the wavenumber space, and the anomalies do not vanish if the structural periodicity is locally collapsed. This implies that the Wood anomalies should be taken into account in the discretization. The present approach uses the pseudo-periodic Fourier transform (PPFT) [15] to consider the discretization scheme in the wavenumber space. Let $f(x)$ be a function of x, and d be a positive real constant. Then the transform is defined by:

$$\overline{f}(x;\xi) = \sum_{m=-\infty}^{\infty} f(x-md)\, e^{imd\xi}, \tag{1}$$

which is implicitly assumed to converge. This transform introduces a transform parameter ξ, and the inverse transform is formally given by integrating on ξ as

$$f(x) = \frac{1}{k_d} \int_{-k_d/2}^{k_d/2} \overline{f}(x;\xi)\, \mathrm{d}\xi \tag{2}$$

where $k_d = 2\pi/d$. The transformed function $\overline{f}(x;\xi)$ has a pseudo-periodic property with the pseudo-period d in terms of x: $\overline{f}(x-md;\xi) = \overline{f}(x;\xi)\exp(-imd\xi)$ for any integer m. Also, $\overline{f}(x;\xi)$ has a periodic property with the period k_d in terms of ξ: $\overline{f}(x;\xi - mk_d) = \overline{f}(x;\xi)$ for any integer m. PPFT is an extension of the periodic Green function [16], which is defined by the radiation field from periodic line-source array with phase shift. The transform parameter ξ relates to the wavenumber when x is the spatial parameter. If the constant d is chosen to be equal with the fundamental period in the x-direction, k_d becomes the inverse lattice constant and the period for the transformed function is given by the Brillouin zone. The Wood anomalies are degenerated to a finite number of points in the Brillouin zone, and the required discretization scheme is comparatively easy to consider. Also, the conventional grating theory based on the Floquet theorem becomes possible to be applied for the scattering problem of imperfectly periodic structures because of the pseudo-periodicity of the transformed fields. The present formulation is based on the rigorous coupled-wave analysis (RCWA) [17, 18] with the help of PPFT.

2. Settings of the problem

This paper considers the electromagnetic scattering problem of a lamellar grating with defects schematically shown in Fig. 1. The grating grooves are parallel to the z-axis, and the direction of original periodicity is parallel to the x-axis. The y-axis is taken so as to be at the center of a ridge, and the top and the bottom of grooves are denoted by $y = h_s$ and $y = h_c$, respectively. In the grating layer $h_c < y < h_s$, the structure is uniform in the y- and the z-directions, and the grating profile is specified by the period d, the ridge width a, and the groove depth $t = h_s - h_c$. The structural periodicity is collapsed by removing some ridges. To indicate the removed ridges, we introduce a notation $\mathscr{D}$, which is a finite subset of integers. If an integer n is an element of $\mathscr{D}$, the ridge whose center is at $x = nd$ is removed. The fields are supposed to

be also uniform in the z-direction and have a time-dependence in $\exp(-i\omega t)$. Then the fields are represented by complex vectors depending only on the space variables x and y and two fundamental polarizations are expressed by TE and TM, in which the electric and magnetic fields are respectively perpendicular to the xy-plane. We sometimes denote the z-component of the electric field for TE-polarization and the z-component of the magnetic field for TM-polarization by $\psi(x,y)$ to express both polarizations simultaneously. The substrate is linear isotropic medium with the permittivity ε_c and the permeability μ_c, and the surrounding medium is denoted by the permittivity ε_s and the permeability μ_s. For lossy media, we use complex values for the permittivity and/or the permeability, and the terms concerning to the current densities are eliminated in the following formulation. The permittivity distribution $\varepsilon(x,y)$ and the permeability distribution $\mu(x,y)$ are independent of y inside the grating layer $h_c < y < h_s$ and, here, we express them and their reciprocals as follows:

$$\eta(x) = q_g^{(\eta)}(x) + q_d^{(\eta)}(x) \tag{3}$$

$$\frac{1}{\eta(x)} = r_g^{(\eta)}(x) + r_d^{(\eta)}(x) \tag{4}$$

for $\eta = \varepsilon, \mu$, where

$$q_g^{(\eta)}(x) = \eta_s + (\eta_c - \eta_s) \sum_{l=-\infty}^{\infty} u(x - l\,d) \tag{5}$$

$$q_d^{(\eta)}(x) = -(\eta_c - \eta_s) \sum_{l \in \mathscr{D}} u(x - l\,d) \tag{6}$$

$$r_g^{(\eta)}(x) = \frac{1}{\eta_s} + \left(\frac{1}{\eta_c} - \frac{1}{\eta_s}\right) \sum_{l=-\infty}^{\infty} u(x - l\,d) \tag{7}$$

$$r_d^{(\eta)}(x) = -\left(\frac{1}{\eta_c} - \frac{1}{\eta_s}\right) \sum_{l \in \mathscr{D}} u(x - l\,d) \tag{8}$$

$$u(x) = \begin{cases} 1 & \text{for } |x| \le a/2 \\ 0 & \text{for } |x| > a/2 \end{cases}. \tag{9}$$

The functions $q_g^{(\eta)}(x)$ and $r_g^{(\eta)}(x)$ give the distributions of perfectly periodic structure, and the functions $q_d^{(\eta)}(x)$ and $r_d^{(\eta)}(x)$ correspond to the defects. The incident field is supposed to illuminate the gratings from the upper or lower regions and there exists no source inside the grating layer $h_c < y < h_s$.

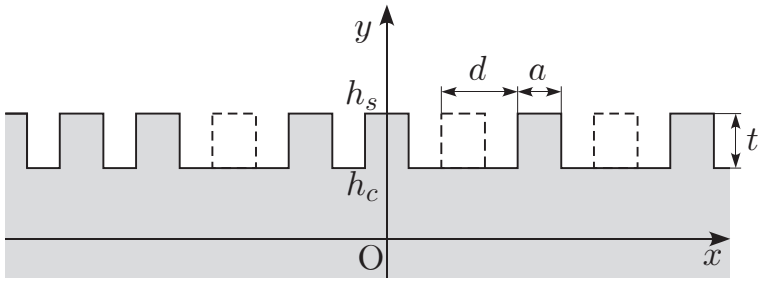

Fig. 1. Lamellar grating with defects.

3. Formulation

First, we consider the TE-polarized fields in the grating layer $h_c < y < h_s$, which are described by

$$\frac{\partial}{\partial x} H_y(x,y) - \frac{\partial}{\partial y} H_x(x,y) = -i\omega D_z(x,y) \tag{10}$$

$$\frac{\partial}{\partial y} E_z(x,y) = i\omega B_x(x,y) \tag{11}$$

$$\frac{\partial}{\partial x} E_z(x,y) = -i\omega B_y(x,y) \tag{12}$$

$$D_z(x,y) = \left(q_g^{(\varepsilon)}(x) + q_d^{(\varepsilon)}(x)\right) E_z(x,y) \tag{13}$$

$$H_x(x,y) = \left(r_g^{(\mu)}(x) + r_d^{(\mu)}(x)\right) B_x(x,y) \tag{14}$$

$$B_y(x,y) = \left(q_g^{(\mu)}(x) + q_d^{(\mu)}(x)\right) H_y(x,y). \tag{15}$$

Equations (10)–(12) come from the Maxwell curl equations, and the constitutive relations yield Eqs. (13)–(15) though they are arranged so as not to include products of two functions with concurrent discontinuities. We apply PPFT to Eqs. (10)–(15), and we may obtain the following relations:

$$\frac{\partial}{\partial x} \overline{H}_y(x;\xi,y) - \frac{\partial}{\partial y} \overline{H}_x(x;\xi,y) = -i\omega \overline{D}_z(x;\xi,y) \tag{16}$$

$$\frac{\partial}{\partial y} \overline{E}_z(x;\xi,y) = i\omega \overline{B}_x(x;\xi,y) \tag{17}$$

$$\frac{\partial}{\partial x} \overline{E}_z(x;\xi,y) = -i\omega \overline{B}_y(x;\xi,y) \tag{18}$$

$$\overline{D}_z(x;\xi,y) = q_g^{(\varepsilon)}(x)\overline{E}_z(x;\xi,y) + \frac{1}{k_d}\int_{-k_d/2}^{k_d/2} \overline{q}_d^{(\varepsilon)}(x;\xi-\xi')\overline{E}_z(x;\xi',y)\,\mathrm{d}\xi' \tag{19}$$

$$\overline{H}_x(x;\xi,y) = r_g^{(\mu)}(x)\overline{B}_x(x;\xi,y) + \frac{1}{k_d}\int_{-k_d/2}^{k_d/2} \overline{r}_d^{(\mu)}(x;\xi-\xi')\overline{B}_x(x;\xi',y)\,\mathrm{d}\xi' \tag{20}$$

$$\overline{B}_y(x;\xi,y) = q_g^{(\mu)}(x)\overline{H}_y(x;\xi,y) + \frac{1}{k_d}\int_{-k_d/2}^{k_d/2} \overline{q}_d^{(\mu)}(x;\xi-\xi')\overline{H}_y(x;\xi',y)\,\mathrm{d}\xi'. \tag{21}$$

Since the transformed fields are pseudo-periodic in terms of x, they can be approximately expanded in the truncated generalized Fourier series. For example, the z-component of electric field is written as

$$\overline{E}_z(x;\xi,y) = \sum_{n=-N}^{N} \overline{E}_{z,n}(\xi,y)\, e^{i\alpha_n(\xi)x} \tag{22}$$

with

$$\alpha_n(\xi) = \xi + nk_d \tag{23}$$

where N denotes the truncation order and $\overline{E}_{z,n}(\xi,y)$ are the nth-order coefficients. To treat the coefficients systematically, we introduce $(2N+1)\times 1$ column matrices; for example, the coefficients of $\overline{E}_z(x;\xi,y)$ are expressed by a column matrix $\overline{\boldsymbol{e}}_z(\xi,y)$ in such a way that its nth-components are given by $\overline{E}_{z,n}(\xi,y)$. Also, supposing that $f(x)$ is a periodic function with period

d, $[\![f]\!]$ denotes the Toeplitz matrix generated by the Fourier coefficients of $f(x)$, in such a way that their (n,m)-entries are given by

$$([\![f]\!])_{n,m} = \frac{1}{d}\int_{-d/2}^{d/2} f(x)\, e^{-i(n-m)k_d x}\,\mathrm{d}x. \tag{24}$$

Similarly, if $\overline{g}(x;\xi)$ is a transformed function that is pseudo-periodic in terms of x, $[\![\overline{g}]\!](\xi)$ denotes the Toeplitz matrix generated by the generalized Fourier coefficients of $\overline{g}(x;\xi)$, in such a way that their (n,m)-entries are

$$([\![\overline{g}]\!](\xi))_{n,m} = \frac{1}{d}\int_{-d/2}^{d/2} \overline{g}(x;\xi)\, e^{-i\alpha_{n-m}(\xi)x}\,\mathrm{d}x. \tag{25}$$

Then Eqs. (16)–(21) yield the following relations:

$$i\overline{\boldsymbol{X}}(\xi)\,\overline{\boldsymbol{h}}_y(\xi,y) - \frac{\partial}{\partial y}\overline{\boldsymbol{h}}_x(\xi,y) = -i\omega\,\overline{\boldsymbol{d}}_z(\xi,y) \tag{26}$$

$$\frac{\partial}{\partial y}\overline{\boldsymbol{e}}_z(\xi,y) = i\omega\,\overline{\boldsymbol{b}}_x(\xi,y) \tag{27}$$

$$i\overline{\boldsymbol{X}}(\xi)\,\overline{\boldsymbol{e}}_z(\xi,y) = -i\omega\,\overline{\boldsymbol{b}}_y(\xi,y) \tag{28}$$

$$\overline{\boldsymbol{d}}_z(\xi,y) = [\![q_g^{(\varepsilon)}]\!]\,\overline{\boldsymbol{e}}_z(\xi,y) + \frac{1}{k_d}\int_{-k_d/2}^{k_d/2} [\![\overline{q}_d^{(\varepsilon)}]\!](\xi-\xi')\,\overline{\boldsymbol{e}}_z(\xi',y)\,\mathrm{d}\xi' \tag{29}$$

$$\overline{\boldsymbol{h}}_x(\xi,y) = [\![r_g^{(\mu)}]\!]\,\overline{\boldsymbol{b}}_x(\xi,y) + \frac{1}{k_d}\int_{-k_d/2}^{k_d/2} [\![\overline{r}_d^{(\mu)}]\!](\xi-\xi')\,\overline{\boldsymbol{b}}_x(\xi',y)\,\mathrm{d}\xi' \tag{30}$$

$$\overline{\boldsymbol{b}}_y(\xi,y) = [\![q_g^{(\mu)}]\!]\,\overline{\boldsymbol{h}}_y(\xi,y) + \frac{1}{k_d}\int_{-k_d/2}^{k_d/2} [\![\overline{q}_d^{(\mu)}]\!](\xi-\xi')\,\overline{\boldsymbol{h}}_y(\xi',y)\,\mathrm{d}\xi' \tag{31}$$

where $\overline{\boldsymbol{X}}(\xi)$ denotes a diagonal matrix whose nth-diagonal components are $\alpha_n(\xi)$. Since the right-hand sides of Eqs. (19)–(21) consist of the products of periodic or pseudo-periodic functions with no concurrent jump discontinuities, the Laurent rule [19] has been used to derive Eqs. (29)–(31).

Equations (26)–(31) that relate the generalized Fourier coefficients of the fields have to be satisfied for arbitrary $\xi \in (-k_d/2, k_d/2]$. However, we introduce here a discretization in the transform parameter ξ for numerical purposes. We take L sample points, and suppose that the coefficients satisfy Eqs. (26)–(31) at these sample points. Also the integrations in Eqs. (29)–(31) are approximated by an appropriate numerical integration scheme using the same sample points. Let $\{\xi_l\}_{l=1}^{L}$ and $\{w_l\}_{l=1}^{L}$ be the sample points and the weights chosen by an appropriate numerical integration scheme. Then we may obtain the following relations:

$$i\widetilde{\boldsymbol{X}}\,\widetilde{\boldsymbol{h}}_y(y) - \frac{\mathrm{d}}{\mathrm{d}y}\widetilde{\boldsymbol{h}}_x(y) = -i\omega\,\widetilde{\boldsymbol{d}}_z(y) \tag{32}$$

$$\frac{\mathrm{d}}{\mathrm{d}y}\widetilde{\boldsymbol{e}}_z(y) = i\omega\,\widetilde{\boldsymbol{b}}_x(y) \tag{33}$$

$$i\widetilde{\boldsymbol{X}}\,\widetilde{\boldsymbol{e}}_z(y) = -i\omega\,\widetilde{\boldsymbol{b}}_y(y) \tag{34}$$

$$\widetilde{\boldsymbol{d}}_z(y) = \widetilde{\boldsymbol{Q}}^{(\varepsilon)}\,\widetilde{\boldsymbol{e}}_z(y) \tag{35}$$

$$\widetilde{\boldsymbol{h}}_x(y) = \widetilde{\boldsymbol{R}}^{(\mu)}\,\widetilde{\boldsymbol{b}}_x(y) \tag{36}$$

$$\widetilde{\boldsymbol{b}}_y(y) = \widetilde{\boldsymbol{Q}}^{(\mu)}\,\widetilde{\boldsymbol{h}}_y(y) \tag{37}$$

where $\widetilde{\boldsymbol{e}}_z(y)$ denotes a column matrix generated by the generalized Fourier coefficients of $\overline{E}_z(x;\xi,y)$ and the coefficients of the other field components are expressed in the same way. The matrices in the equations are defined as follows:

$$\widetilde{\boldsymbol{e}}_z(y) = \begin{pmatrix} \overline{\boldsymbol{e}}_z(\xi_1,y) \\ \vdots \\ \overline{\boldsymbol{e}}_z(\xi_L,y) \end{pmatrix} \tag{38}$$

$$\widetilde{\boldsymbol{X}} = \begin{pmatrix} \overline{\boldsymbol{X}}(\xi_1) & & \boldsymbol{0} \\ & \ddots & \\ \boldsymbol{0} & & \overline{\boldsymbol{X}}(\xi_L) \end{pmatrix} \tag{39}$$

$$\widetilde{\boldsymbol{Q}}^{(\upsilon)} = \begin{pmatrix} \boldsymbol{Q}_{1,1}^{(\upsilon)} & \cdots & \boldsymbol{Q}_{1,L}^{(\upsilon)} \\ \vdots & \ddots & \vdots \\ \boldsymbol{Q}_{L,1}^{(\upsilon)} & \cdots & \boldsymbol{Q}_{L,L}^{(\upsilon)} \end{pmatrix} \tag{40}$$

$$\widetilde{\boldsymbol{R}}^{(\upsilon)} = \begin{pmatrix} \boldsymbol{R}_{1,1}^{(\upsilon)} & \cdots & \boldsymbol{R}_{1,L}^{(\upsilon)} \\ \vdots & \ddots & \vdots \\ \boldsymbol{R}_{L,1}^{(\upsilon)} & \cdots & \boldsymbol{R}_{L,L}^{(\upsilon)} \end{pmatrix} \tag{41}$$

$$\boldsymbol{Q}_{l,l'}^{(\upsilon)} = \delta_{l,l'} [\![q_g^{(\upsilon)}]\!] + \frac{w_{l'}}{k_d} [\![\overline{q}_d^{(\upsilon)}]\!] (\xi_l - \xi_{l'}) \tag{42}$$

$$\boldsymbol{R}_{l,l'}^{(\upsilon)} = \delta_{l,l'} [\![r_g^{(\upsilon)}]\!] + \frac{w_{l'}}{k_d} [\![\overline{r}_d^{(\upsilon)}]\!] (\xi_l - \xi_{l'}) \tag{43}$$

for $\upsilon = \varepsilon, \mu$, where $\delta_{l,l'}$ denotes the Kronecker delta.

Equations (32)–(37) yield the following coupled second-order differential-equation set:

$$\frac{\mathrm{d}^2}{\mathrm{d}y^2} \widetilde{\boldsymbol{e}}_z(y) = -\widetilde{\boldsymbol{C}}_g^{(e)} \widetilde{\boldsymbol{e}}_z(y) \tag{44}$$

with the matrix of coefficients:

$$\widetilde{\boldsymbol{C}}_g^{(e)} = \widetilde{\boldsymbol{R}}^{(\mu)^{-1}} \left(\omega^2 \widetilde{\boldsymbol{Q}}^{(\varepsilon)} - \widetilde{\boldsymbol{X}} \widetilde{\boldsymbol{Q}}^{(\mu)^{-1}} \widetilde{\boldsymbol{X}} \right). \tag{45}$$

The coupled differential equation set (44) can be solved as eigenvalue-eigenvector problems because the matrix of coefficients $\widetilde{\boldsymbol{C}}_g^{(e)}$ is constant. Here, we denote the square root of the nth-eigenvalue and the associated eigenvector of $\widetilde{\boldsymbol{C}}_g^{(e)}$ by $\beta_{g,n}^{(e)}$ and $\boldsymbol{p}_{g,n}^{(e)}$, respectively, where the sign of square root is taken in such a way that $\Im(\beta_{g,n}^{(e)}) > 0$ when $\Im(\beta_{g,n}^{(e)}) \neq 0$ and that $\Re(\beta_{g,n}^{(e)}) > 0$ when $\Im(\beta_{g,n}^{(e)}) = 0$. Then, from Eqs. (33), (36) and (44), the general solutions for $\widetilde{\boldsymbol{e}}_z(y)$ and $\widetilde{\boldsymbol{h}}_x(y)$ are written in the following form:

$$\begin{pmatrix} \widetilde{\boldsymbol{e}}_z(y) \\ \widetilde{\boldsymbol{h}}_x(y) \end{pmatrix} = \boldsymbol{\Xi}_g^{(e)} \begin{pmatrix} \widetilde{\boldsymbol{a}}_g^{(e,-)}(y) \\ \widetilde{\boldsymbol{a}}_g^{(e,+)}(y) \end{pmatrix} \tag{46}$$

with

$$\boldsymbol{\Xi}_g^{(e)} = \begin{pmatrix} \widetilde{\boldsymbol{P}}_g^{(e)} & \widetilde{\boldsymbol{P}}_g^{(e)} \\ -\frac{1}{\omega} \widetilde{\boldsymbol{R}}^{(\mu)} \widetilde{\boldsymbol{P}}_g^{(e)} \widetilde{\boldsymbol{Y}}_g^{(e)} & \frac{1}{\omega} \widetilde{\boldsymbol{R}}^{(\mu)} \widetilde{\boldsymbol{P}}_g^{(e)} \widetilde{\boldsymbol{Y}}_g^{(e)} \end{pmatrix} \tag{47}$$

$$\widetilde{\boldsymbol{P}}_g^{(e)} = \begin{pmatrix} \boldsymbol{p}_{g,1}^{(e)} & \cdots & \boldsymbol{p}_{g,L(2N+1)}^{(e)} \end{pmatrix} \tag{48}$$

$$\left(\widetilde{\boldsymbol{Y}}_g^{(e)}\right)_{n,m} = \delta_{n,m}\beta_{g,n}^{(e)}. \tag{49}$$

Two $L(2N+1)\times 1$ column matrices $\widetilde{\boldsymbol{a}}_g^{(e,-)}(y)$ and $\widetilde{\boldsymbol{a}}_g^{(e,+)}(y)$ give the amplitudes of eigenmodes propagating in the negative and positive y-directions, respectively. We include the y-dependence of each amplitude, and their y-dependences are expressed by

$$\widetilde{\boldsymbol{a}}_g^{(e,\pm)}(y) = \widetilde{\boldsymbol{A}}_g^{(e)}(\pm(y-y'))\,\widetilde{\boldsymbol{a}}_g^{(e,\pm)}(y') \tag{50}$$

with

$$\left(\widetilde{\boldsymbol{A}}_g^{(e)}(y)\right)_{n,m} = \delta_{n,m}e^{i\beta_{g,n}^{(e)}y} \tag{51}$$

for $h_c < y, y' < h_s$.

Outside the grating layer ($y > h_s$ and $y < h_c$), the permittivity and the permeability are constant, and the electromagnetic fields can be approximately expressed by the truncated Rayleigh expansions [16]. Each term of this expansion represents a plane wave, and we include the exponential y-dependence of each term in the Rayleigh coefficient. Here, the regions $y > h_s$ and $y < h_c$ are specified by s and c, respectively, and the wavenumber in each region is denoted by $k_r = \omega(\varepsilon_r\mu_r)^{1/2}$ for $r = s,c$. The relations between the generalized Fourier coefficients of the field components and the amplitudes of the plane-waves can be written in the following forms:

$$\begin{pmatrix} \widetilde{\boldsymbol{e}}_z(y) \\ \widetilde{\boldsymbol{h}}_x(y) \end{pmatrix} = \boldsymbol{\Xi}_r^{(e)} \begin{pmatrix} \widetilde{\boldsymbol{a}}_r^{(e,-)}(y) \\ \widetilde{\boldsymbol{a}}_r^{(e,+)}(y) \end{pmatrix} \tag{52}$$

with

$$\boldsymbol{\Xi}_r^{(e)} = \begin{pmatrix} \boldsymbol{I} & \boldsymbol{I} \\ -\frac{1}{\omega\mu_r}\widetilde{\boldsymbol{Y}}_r & \frac{1}{\omega\mu_r}\widetilde{\boldsymbol{Y}}_r \end{pmatrix} \tag{53}$$

$$\left(\widetilde{\boldsymbol{Y}}_r\right)_{n,m} = \delta_{n,m}\sqrt{{k_r}^2 - (\widetilde{\boldsymbol{X}})_{n,n}} \tag{54}$$

for $r = s,c$, where $\boldsymbol{I}$ denotes the identity matrix.

For the TM-polarized fields, the same manipulation as with the TE-polarized case can be applied. Then the general solutions for the generalized Fourier coefficients of $\overline{H}_z(x;\xi,y)$ and $\overline{E}_x(x;\xi,y)$ are expressed in the same forms with Eqs. (46) and (52), though we specify below the matrices by the superscript h for the TM-polarization instead of those with superscript e for the TE-polarization. The matrices $\widetilde{\boldsymbol{P}}_g^{(h)}$, $\widetilde{\boldsymbol{Y}}_g^{(h)}$, and $\widetilde{\boldsymbol{A}}_g^{(h)}(y)$ that appear below are defined by Eqs. (48), (49), and (51) but with the eigenvalues and eigenvectors of the matrix $\widetilde{\boldsymbol{C}}_g^{(h)} = \widetilde{\boldsymbol{R}}^{(\varepsilon)^{-1}}(\omega^2\widetilde{\boldsymbol{Q}}^{(\mu)} - \widetilde{\boldsymbol{X}}\,\widetilde{\boldsymbol{Q}}^{(\varepsilon)^{-1}}\widetilde{\boldsymbol{X}})$.

The general solutions separately obtained in the grating layer and two homogeneous regions s and c can be matched at the top and the bottom of grooves $y = h_r$ ($r = s,c$) by using the boundary conditions. Considering the continuities of the tangential components of the fields, the amplitudes of the eigenmodes inside the grating layer are related to those of the plane-waves outside the layer by

$$\begin{pmatrix} \widetilde{\boldsymbol{a}}_g^{(f,-)}(h_r) \\ \widetilde{\boldsymbol{a}}_g^{(f,+)}(h_r) \end{pmatrix} = \begin{pmatrix} \widetilde{\boldsymbol{G}}_r^{(f,+)} & \widetilde{\boldsymbol{G}}_r^{(f,-)} \\ \widetilde{\boldsymbol{G}}_r^{(f,-)} & \widetilde{\boldsymbol{G}}_r^{(f,+)} \end{pmatrix} \begin{pmatrix} \widetilde{\boldsymbol{a}}_r^{(f,-)}(h_r) \\ \widetilde{\boldsymbol{a}}_r^{(f,+)}(h_r) \end{pmatrix} \tag{55}$$

with

$$\widetilde{\boldsymbol{G}}_r^{(e,\pm)} = \frac{1}{2}\left(\widetilde{\boldsymbol{P}}_g^{(e)^{-1}} \pm \frac{1}{\mu_r}\widetilde{\boldsymbol{Y}}_g^{(e)^{-1}}\widetilde{\boldsymbol{P}}_g^{(e)^{-1}}\widetilde{\boldsymbol{R}}^{(\mu)^{-1}}\widetilde{\boldsymbol{Y}}_r\right) \tag{56}$$

$$\widetilde{\boldsymbol{G}}_r^{(h,\pm)} = \frac{1}{2}\left(\widetilde{\boldsymbol{P}}_g^{(h)^{-1}} \pm \frac{1}{\varepsilon_r}\widetilde{\boldsymbol{Y}}_g^{(h)^{-1}}\widetilde{\boldsymbol{P}}_g^{(h)^{-1}}\widetilde{\boldsymbol{R}}^{(\varepsilon)^{-1}}\widetilde{\boldsymbol{Y}}_r\right) \tag{57}$$

for $f = e,h$. Using the exponential y-dependence of the amplitudes expressed by Eq. (50) also, the amplitudes of the outgoing plane-waves and the eigenmodes inside the grating layer are related to the those of the incoming plane-waves as

$$\begin{pmatrix} \widetilde{\boldsymbol{a}}_s^{(f,+)}(h_s) \\ \widetilde{\boldsymbol{a}}_c^{(f,-)}(h_c) \\ \widetilde{\boldsymbol{a}}_g^{(f,-)}(h_s) \\ \widetilde{\boldsymbol{a}}_g^{(f,+)}(h_c) \end{pmatrix} = \begin{pmatrix} \widetilde{\boldsymbol{S}}_{11}^{(f)} & \widetilde{\boldsymbol{S}}_{12}^{(f)} \\ \widetilde{\boldsymbol{S}}_{21}^{(f)} & \widetilde{\boldsymbol{S}}_{22}^{(f)} \\ \widetilde{\boldsymbol{S}}_{31}^{(f)} & \widetilde{\boldsymbol{S}}_{32}^{(f)} \\ \widetilde{\boldsymbol{S}}_{41}^{(f)} & \widetilde{\boldsymbol{S}}_{42}^{(f)} \end{pmatrix} \begin{pmatrix} \widetilde{\boldsymbol{a}}_s^{(f,-)}(h_s) \\ \widetilde{\boldsymbol{a}}_c^{(f,+)}(h_c) \end{pmatrix} \tag{58}$$

with

$$\widetilde{\boldsymbol{S}}_{11}^{(f)} = -\left(\widetilde{\boldsymbol{G}}_s^{(f,+)} - \widetilde{\boldsymbol{A}}_g^{(f)}(t)\,\widetilde{\boldsymbol{G}}_c^{(f,-)}\,\widetilde{\boldsymbol{G}}_c^{(f,+)^{-1}}\widetilde{\boldsymbol{A}}_g^{(f)}(t)\,\widetilde{\boldsymbol{G}}_s^{(f,-)}\right)^{-1} \left(\widetilde{\boldsymbol{G}}_s^{(f,-)} - \widetilde{\boldsymbol{A}}_g^{(f)}(t)\,\widetilde{\boldsymbol{G}}_c^{(f,-)}\,\widetilde{\boldsymbol{G}}_c^{(f,+)^{-1}}\widetilde{\boldsymbol{A}}_g^{(f)}(t)\,\widetilde{\boldsymbol{G}}_s^{(f,+)}\right) \tag{59}$$

$$\widetilde{\boldsymbol{S}}_{12}^{(f)} = \left(\widetilde{\boldsymbol{G}}_s^{(f,+)} - \widetilde{\boldsymbol{A}}_g^{(f)}(t)\,\widetilde{\boldsymbol{G}}_c^{(f,-)}\,\widetilde{\boldsymbol{G}}_c^{(f,+)^{-1}}\widetilde{\boldsymbol{A}}_g^{(f)}(t)\,\widetilde{\boldsymbol{G}}_s^{(f,-)}\right)^{-1} \widetilde{\boldsymbol{A}}_g^{(f)}(t)\left(\widetilde{\boldsymbol{G}}_c^{(f,+)} - \widetilde{\boldsymbol{G}}_c^{(f,-)}\,\widetilde{\boldsymbol{G}}_c^{(f,+)^{-1}}\widetilde{\boldsymbol{G}}_c^{(f,-)}\right) \tag{60}$$

$$\widetilde{\boldsymbol{S}}_{21}^{(f)} = \widetilde{\boldsymbol{G}}_c^{(f,+)^{-1}}\widetilde{\boldsymbol{A}}_g^{(f)}(t)\left(\widetilde{\boldsymbol{G}}_s^{(f,+)} + \widetilde{\boldsymbol{G}}_s^{(f,-)}\widetilde{\boldsymbol{S}}_{11}^{(f)}\right) \tag{61}$$

$$\widetilde{\boldsymbol{S}}_{22}^{(f)} = -\widetilde{\boldsymbol{G}}_c^{(f,+)^{-1}}\left(\widetilde{\boldsymbol{G}}_c^{(f,-)} - \widetilde{\boldsymbol{A}}_g^{(f)}(t)\,\widetilde{\boldsymbol{G}}_s^{(f,-)}\widetilde{\boldsymbol{S}}_{12}^{(f)}\right) \tag{62}$$

$$\widetilde{\boldsymbol{S}}_{31}^{(f)} = \widetilde{\boldsymbol{G}}_s^{(f,+)} + \widetilde{\boldsymbol{G}}_s^{(f,-)}\widetilde{\boldsymbol{S}}_{11}^{(f)} \tag{63}$$

$$\widetilde{\boldsymbol{S}}_{32}^{(f)} = \widetilde{\boldsymbol{G}}_s^{(f,-)}\widetilde{\boldsymbol{S}}_{12}^{(f)} \tag{64}$$

$$\widetilde{\boldsymbol{S}}_{41}^{(f)} = \widetilde{\boldsymbol{G}}_c^{(f,-)}\widetilde{\boldsymbol{S}}_{21}^{(f)} \tag{65}$$

$$\widetilde{\boldsymbol{S}}_{42}^{(f)} = \widetilde{\boldsymbol{G}}_c^{(f,+)} + \widetilde{\boldsymbol{G}}_c^{(f,-)}\widetilde{\boldsymbol{S}}_{22}^{(f)}. \tag{66}$$

The amplitudes of the incoming plane-waves are calculated from the incident fields that should be known, and the scattered fields are obtained from the amplitudes appeared in the left-hand side of Eq. (58).

4. Numerical experiments

To validate the present formulation, we consider specific examples excited by a line-source situated parallel to the z-axis at $(x,y) = (x_0,y_0)$ where $y_0 > h_s$. The incident field is then expressed as

$$\psi^{(i)}(x,y) = H_0^{(1)}(k_s\,\rho\,(x-x_0,y-y_0)) \tag{67}$$

where $H_0^{(1)}$ denotes the zeroth-order Hankel function of the first kind and $\rho\,(x,y) = \left(x^2+y^2\right)^{1/2}$. The grating parameters are chosen as follows: $d = 0.6\,\lambda_0$, $a = 0.6\,d$, $h_s = 0$, $h_c = -0.5\,d$, $\varepsilon_s = \varepsilon_0$,

$\varepsilon_c = (1.3+i7.6)^2\,\varepsilon_0$, and $\mu_s = \mu_c = \mu_0$. We also set the position of line-source at $(x,y) = (0,2d)$ and the observation point for convergence tests at $(x,y) = (0,d)$.

First, we consider the grating for $\mathscr{D} = \{0\}$, in which only one ridge with the center at $x = 0$ is removed from the perfectly periodic grating. Figure 2(a) shows the obtained results of the field intensity at the observation point as a function of the number of sample points L. The truncation order for each generalized Fourier series expansion is set to $N = 5$ for this computation. The dotted curves are the results of the trapezoidal scheme that uses equidistant sample points and equal weights. The trapezoidal scheme is known to usually provide a fast convergence for the integration of smooth periodic function over one period, but they converge very slowly. This implies that the spectra under consideration may be non-smooth. The fields in perfectly periodic structures are known to be non-smooth at the Wood-Rayleigh anomalies in the wavenumber space. We expect the spectra of fields in imperfectly periodic structure have a similar singularity to those for the periodic structure without defect, and apply here the same discretization scheme proposed for the perfectly periodic grating with the line-source excitation in Ref. [15]. The Wood-Rayleigh anomalies occur when the diffracted field of a spectral order propagates along the grating surface, and this implies that the transform parameter ξ has to satisfy $\alpha_n(\xi) = \pm k_s, k_c$ at the anomalies. Since we consider here a lossy material for the substrate, the anomalies degenerate at two points $\xi = \pm 0.4\,k_d$ in the Brillouin zone. We split the Brillouin zone at these points and apply the commonly used numerical integration schemes for each subinterval. This discretization scheme is also valid for another imperfectly periodic structure, in which some circular cylinders are located near the periodic cylinder array [20]. The solid curves in Fig. 2(a) are the result of the double exponential scheme [21, 22] applying for the subintervals, and show significant improvement of convergence. The convergences with respect to the truncation order N are shown in Fig. 2(b). The values are computed for $L = 80$ and the sample points and weights are determined by the double exponential scheme applying for the subintervals. It is observed that the convergences are fast. Figure 3 shows the field intensities computed with $L = 80$ and $N = 5$ by changing the observation point. The position of grating surface is indicated by the dashed line. The fields decay rapidly inside the substrate because the substrate is assumed to be a conducting material. The field for TE-polarization does not propagate into the narrow grooves because of the cutoff. Therefore, the horizontal interference fringes observed in Fig. 3(a) are similar to those for the plane conducting plate though the phase shift is also observed near

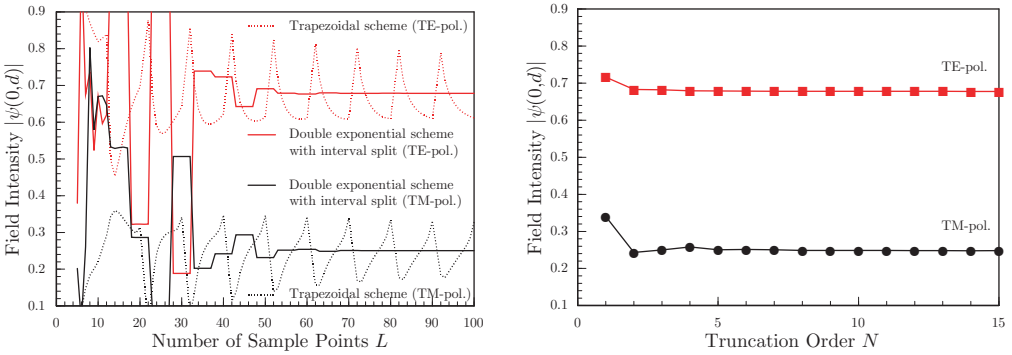

(a) Convergence on the number of sample points L

(b) Convergence on the truncation order N

Fig. 2. Convergence of the field intensities at $(x,y) = (0,d)$ for a lamellar grating with a defect for a line-source excitation.

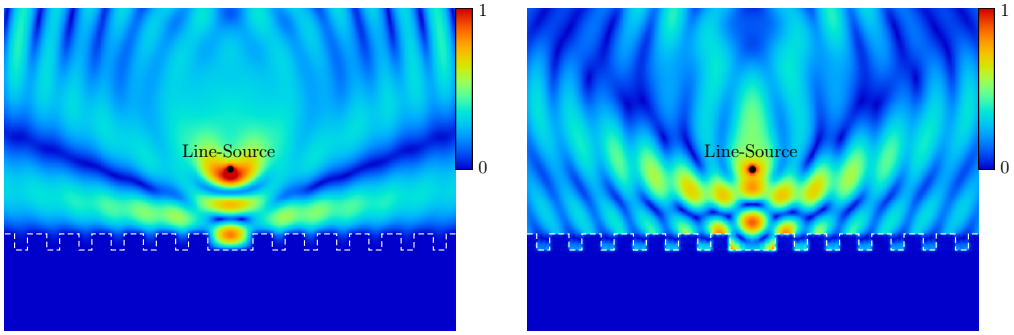

(a) TE-polarization (b) TM-polarization

Fig. 3. Field intensities near a lamellar grating with a defect for the line-source excitation.

the defect. For the TM-polarization, the fields can propagate into the narrow grooves and the vertical fringes are stronger than these for the TE-polarization.

Next, we consider the grating in which five ridges are removed ($\mathscr{D} = \{-3,0,2,3,5\}$). Figure 4 shows the results of the same convergence tests with Fig. 2. The convergence seems to be similar to the single defect case, and the number of defects does not greatly affect the convergence speed. Also, the field intensities computed with $L = 80$ and $N = 5$ are shown in Fig. 5. The obtained results seems to be proper. We examine the reciprocal property to verify the present formulation. Here, we define the reciprocity error for two points (x_p, y_p) and (x_q, y_q) by

$$\sigma(x_p,y_p;x_q,y_q) = \frac{\left|\psi(x_p,y_p;x_q,y_q) - \psi(x_q,y_q;x_p,u_p)\right|}{\left|\psi(x_p,y_p;x_q,y_q)\right|} \tag{68}$$

where $\psi(x_p,y_p;x_q,y_q)$ denotes the field observed at (x_p,y_p) for a line-source located at (x_q,y_q). The reciprocity theorem requires that this function is zero when both (x_p,y_p) and (x_q,y_q) are located in the surrounding medium. We fix one point at $(x_p,y_p) = (0,2d)$ and the other point (x_q,y_q) is moved on the line $y = d$. The reciprocity errors at 101 equidistant points in $-7d \leq x \leq$

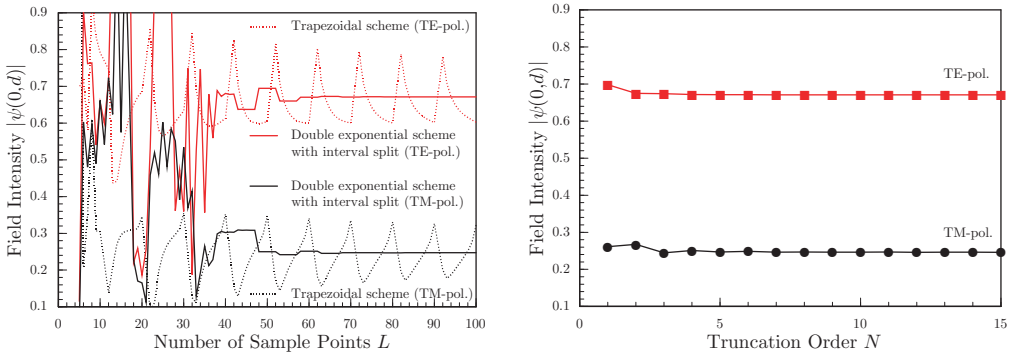

(a) Convergence on the number of sample points L (b) Convergence on the truncation order N

Fig. 4. Convergence of the field intensities at $(x,y) = (0,d)$ for a lamellar grating with five defects for a line-source excitation.

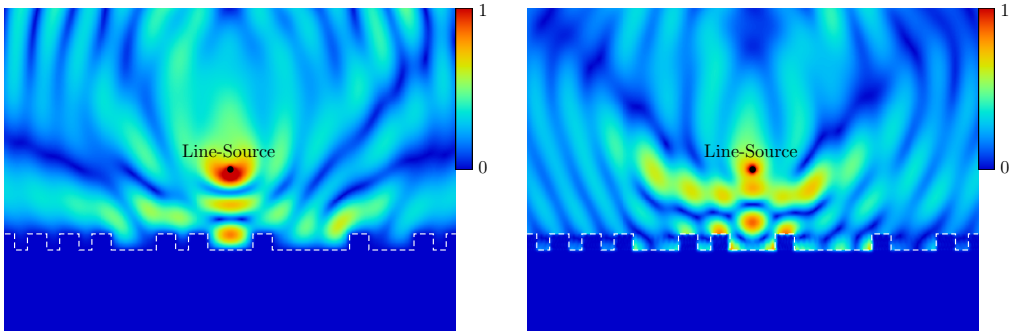

(a) TE-polarization (b) TM-polarization

Fig. 5. Field intensities near a lamellar grating with five defects for the line-source excitation.

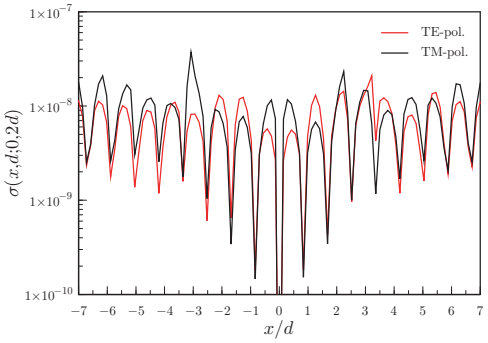

Fig. 6. Numerical results of the reciprocity test for a lamellar grating with five defects for the line-source excitation.

$7\,d$ are calculated with $L = 80$ and $N = 5$ in the standard double-precision arithmetic, and Fig. 6 shows the obtained results. The largest values are about 2.1×10^{-8} for the TE-polarization and 3.7×10^{-8} for the TM-polarization, and the reciprocity relation is well satisfied.

5. Concluding remarks

This paper has presented a spectral-domain formulation of the two-dimensional electromagnetic scattering from lamellar gratings with defects. The readers may understand that the formulation presented in Sec. 3 is almost the same as the widely used RCWA. We introduced PPFT to the fields in the imperfectly periodic structures, and RCWA was then possible to be applied because the transformed fields that have a pseudo-periodic property. The main difficulty on the spectral-domain analysis is generally summarized to the discretization scheme on the wavenumber, and PPFT makes it possible to consider the arrangement of sample points only inside the Brillouin zone. We have shown some numerical results for gratings made of conducting material for a line-source excitation. The Brillouin zone is splitted at the Wood-Rayleigh anomalies and the double exponential scheme is applied for each subinterval to determine the sample points and weights. This simple discretization scheme provided good convergences, and the convergence speed did not depend on the number of defects. The present formulation was also validated by the reciprocity test.

For the practical applications, the plane-wave incidence problem is also important though this paper showed the results for the line-source excitation problem. The plane-wave does not have a continuous spectrum and becomes the Dirac delta in the wavenumber space. Some equations then become simpler for lack of generality because the discretization concerning the incident fields is not needed. Contrarily, it seems to be better to decompose the fields into that for the perfectly periodic structures and the residuals, and some additional arrangements are required for the present formulation. Of course it is not difficult, but this paper concentrates on the problem for the incident fields with continuous spectra to show clearly the relationship to the conventional RCWA.

Acknowledgments

This work has been partially supported by the Grant Agency of the Czech Republic (#P205/11/2137), by the Ministry of Education, Yourth and Sport of the Czech Republic (#MSM 6198910016), and by the IT4Innovations Centre of Excellence project, reg. no. CZ.1.05/1.1.00/02.0070.